calculated value was found to be $C_{Df}^2 = 0\ 506$ (calculated)

The factor $\frac{2}{6}\frac{7}{4}$ was derived assuming bodies with vanishingly small blunt noses The case considered here obviously departs from this assumption Reference 1 shows that the optimum value of C_{Df}^2 is a function of Mach number and fineness ratio

The work previously discussed was all carried out under the assumption of inviscid flows Reference 5 discusses the influence of skin friction on the body minimum drag although using several simplifying assumptions The process used in this note can be used to determine the exact viscid plus inviscid minimum drag shapes merely by adding an accurate viscous program to the process of calculating the individual body drags

References

[1] Powers, S A, "Minimum drag bodies of revolution by exact methods," NOR-63-156, Northrop Corp, Norair Div (September 1963)

[2] Powers, S A, "Drag minimization using exact methods," NOR-63 162, Northrop Corp Norair Div (September 1963)

[3] Sommer, S C and Stark, J A, "The effect of bluntness on the drag of spherical-tipped truncated cones of fineness ratio 3 at Mach numbers 1 2 to 7 4," NACA RM A52B13 (1952)

[4] Miele, A, "Optimum slender bodies of revolution in Newtonian flow," Flight Sciences Labs TR 56, Boeing Scientific Research Labs (April 1962)

[5] Miele, A and Cole, J, "A study of optimum slender bodies in hypersonic flow with a variable friction coefficient," Flight Sciences Labs TR 66, Boeing Scientific Research Labs (January 1963)

Variation in Buckle Shape in Cylindrical Shells under External Pressure and Axial Load

W H Horton* and S C Durham†

Stanford University, Stanford, Calif

THE behavior of cylindrical shells under the combined action of internal pressure and axial compression has been studied, both theoretically and experimentally, by many investigators Prescott,[1] analyzing the problem on the basis of small displacement theory, reached the conclusion that there should be a parabolic increase of the critical buckling stress with the dimensionless parameter $\bar{p} = (p/E)(R/t)^2$, where p is the internal pressure, E is Young's modulus, R is the radius of the cylinder, and t is its wall thickness Flügge[2] re-examined the problem and after a comprehensive study reached the conclusion that internal pressure would have negligible effect on the buckling load These theoretical deductions are contradicted by experimental results Thus, Lo, Crate, and Schwartz[3] constructed a large-deflection theory, using the method of von Kármán and Tsien,[4] and showed that under these assumptions buckling load should increase with increasing values of $\bar{p}$ up to $\bar{p} = 0\ 169$ and thereafter remain constant Holmes[5] carried out a series of tests on the behavior of thin-walled cylinders under axial load and internal pressure The cylinders were made of aluminum alloy and were 3 ft in diameter and either 6 or 9 ft in length In his paper Holmes shows the buckle patterns that he obtained for various ratios of circumferential to longitudinal stress He observes that as this ratio increases there is a significant change in the aspect ratio of the buckles Fung

Received January 15 1964 This work was performed for the U S Army Transportation Research Command under Contract DA 44-177-AMC-115(T)

* Director of Laboratories

† Major, U S Air Force

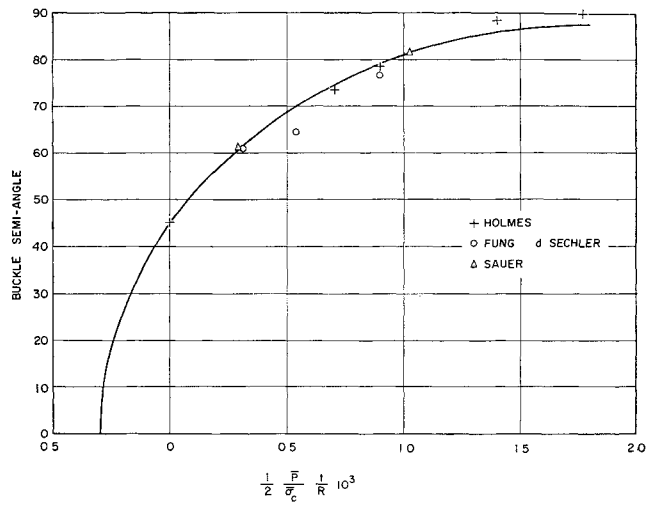

Fig 1 Variation of semiangle of buckle with pressure/stress ratio

and Sechler,[6] in their paper on the buckling of thin-walled circular cylinders under compression and internal pressure, make the same observation These experimenters used aluminum cylinders 3 5 in in diameter, 11 in in length, and having a wall thickness of one thousandth of an inch In a subsequent paper[7] the same authors show results obtained by Suer The same qualitative results are apparent

We have examined the pictorial results given in the forementioned reports and have found that there is a distinct connection between the angle of buckle and the parameter p/σ_c The results of all these experimenters are plotted in Fig 1 It is seen from this figure that if we plot the semiangle of buckle against the ratio p/σ_c we obtain a smooth curve Complete details of the characteristics of the cylindrical shells and the measured semiangles of buckles are given in Table 1 We should emphasize that the various cylinders on which these observations were made were widely different with regard to the R/t ratio Moreover, some specimens were made from aluminum with a Young's modulus of 10×10^6 and others from steel with a Young's modulus of 30×10^6 The variation in L/D was, however, not great

The elliptic curve whose equation is given by

$$\theta = 41\ 665[1\ 17 + 1\ 8 \times 10^3(p/\sigma_c) - 0\ 25 \times 10^6(p/\sigma_c)^2]^{1/2} \text{ deg}$$

appears to be a good approximation to the relationship between the buckle semiangle θ and the pressure/stress ratio p/σ_c

Table 1 Listing of $\frac{1}{2}\ (\bar{p}/\bar{\sigma})\ (t/R) \times 10^3$ vs buckle semiangle

$\frac{1}{2}\frac{\bar{p}}{\bar{\sigma}}\frac{t}{R} \times 10^3$	Semiangle	Source
0 321	61°	Fung and Sechler (Suer), Fig 19a
1 026	81° 30′	Fung and Sechler (Suer), Fig 19b
0 311	60° 57′	Fung and Sechler, Fig 6
0 541	64° 32′	Fung and Sechler, Fig 7
0 900	76° 30′	Fung and Sechler Fig 9
0 705	73° 30′	Holmes, Spec 6 (top)
0 903	78° 30′	Holmes, Spec 6 (bottom)
1 4	88° 30′	Holmes, Spec 5
1 77	90°	Holmes Spec 3

References

[1] Prescott, J, *Applied Elasticity* (Dover Publications, New York, 1946), Chap XVII

[2] Flügge W, *Stresses in Shells* (Springer Verlag, Berlin, 1960), Chap VII

[3] Lo H, Crate, H and Schwartz, E B "Buckling of thin-walled cylinders under axial compression and internal pressure," NACA TN 2021 (January 1950)

[4] von Kármán, T and Tsien, H-S, 'The buckling of thin cylindrical shells under axial compression, J Aeronaut Sci **8**, 303–312 (1941)

[5] Holmes, M, 'Compression tests on thin-walled cylinders," Aeronaut Quart **12**, 150–164 (February–November 1961)

[6] Fung, Y C and Sechler, E E, 'Buckling of thin-walled circular cylinders under axial compression and internal pressure," J Aeronaut Sci **24**, 351–356 (1957)

[7] Fung, Y C and Sechler, E E, "Instability of thin elastic shells," *Structural Mechanics*, edited by J N Goodier and N J Hoff (Pergamon Press, New York, 1960), pp 115–168

Experimental Measurement of Pitot Pressure in the Boundary Layer on a Model in a Hypersonic Gun Tunnel

A J Cable*

The War Office, Royal Armament Research and Development Establishment, Fort Halstead, England

RECENT interest in hypersonic boundary layers has led to the development of instrumentation to measure the pitot pressure in the boundary layer on a model in the (Royal Armament Research and Development Establishment) no 3 Hypersonic Gun Tunnel,[1] which, at its present stage of development, is capable of simulating both full scale Mach numbers and Reynolds numbers for quite large vehicles The flow duration in this tunnel is of the order of 40 msec

The model chosen for exploratory testing was a flat plate with a hemicylindrical leading edge ($\frac{1}{8}$-in radius) that had previously been pressure plotted The model with the small pitot tube for boundary-layer measurements is shown in Fig 1 The pitot was constructed of flattened hypodermic tubing measuring 0 022 in × 0 018 in externally and 0 011 in × 0 009 in internally The tube was brazed to a body containing a Statham type PM 222 TC transducer The body could be moved inside the model to position the pitot tube in the boundary layer from a point 0 1 in from the surface of the model to flush with the surface

The model was tested at a Mach number of 8 4, and the Reynolds number at the pitot position was $6\,2 \times 10^6$ based on freestream conditions and its distance from the leading edge For some of the tests, an externally mounted pitot tube was also used to measure the pitot pressure in the region between the bow shock wave and the limit of movement of the internally mounted pitot tube The boundary layer was traversed at 0 01-in intervals by the internal pitot and at approximately $\frac{1}{4}$-in intervals with the external pitot

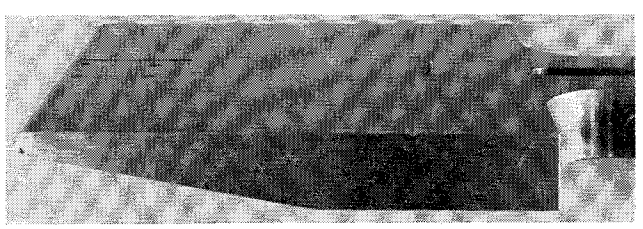

Fig 1 Model showing boundary-layer pitot

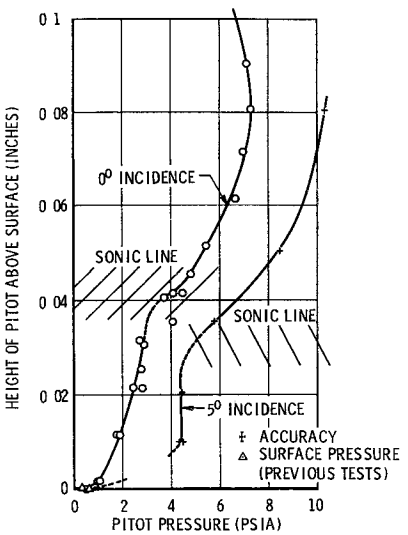

Fig 2 Pitot traverse close to model surface

Figure 2 shows the distribution of pitot pressure in the region between the surface and 0 1 in from the surface for the model at zero and 5° incidence Also indicated are the surface pressures measured in previous tests In each case the surface pitot pressure is close to the surface static pressure It can be seen that the measurements are repeatable except for the region around 0 04 in from the surface at zero incidence On examining schlieren photographs (Fig 3), it was noticed that the shock wave caused by the small pitot tube ended abruptly at about this height This indicated the position of the sonic line in the boundary layer, and it is considered that the nonrepeatability of measurements in this region was caused by the flow being choked locally by the presence of the pitot tube Since the position cannot be measured to a greater accuracy than ±0 005 in from the photographs, the sonic line is shown hatched in Fig 2 A similar effect occurs at incidence but at a lower height

The pitot pressure distribution in the flow between the model surface and bow shock wave (Fig 4) shows that there is a region where the pitot pressure does not vary with height above the surface (0 1–0 4 in at zero incidence) On examining schlieren photographs (e g, Fig 3), it can be seen that this region corresponds to a light region with ill-defined edges This has been interpreted as the entropy layer in previous tests,[2] and a similar interpretation is plausible in this case The extent of the region measured from the schlieren photo-

Fig 3 Schlieren photograph of model at $M = 8\,4$

Received January 13, 1964 British Crown Copyright reserved Published with the permission of the Controller of Her Britannic Majesty's Stationery Office

* Now Supervisor, Launcher Systems Section, von Kármán Gas Dynamics Facility, ARO, Inc (contract operator of the Arnold Engineering Development Center Air Force Systems Command, under U S Air Force Contract No AF 40(600)-1000) Member AIAA